In Situ Lumbar Facet Capsular Ligament Strains Due to Joint Pressure and Residual Strain

Elizabeth Gacek
Department of Biomedical Engineering,
University of Minnesota,
Twin Cities,
Minneapolis, MN 55455

Arin M. Ellingson
Divisions of Physical Therapy and Rehabilitation Science,
Department of Rehabilitation Medicine,
University of Minnesota,
Twin Cities,
Minneapolis, MN 55455

Victor H. Barocas
Department of Biomedical Engineering,
University of Minnesota,
Twin Cities,
Minneapolis, MN 55455

The lumbar facet capsular ligament, which surrounds and limits the motion of each facet joint in the lumbar spine, has been recognized as being mechanically significant and has been the subject of multiple mechanical characterization studies in the past. Those studies, however, were performed on isolated tissue samples and thus could not assess the mechanical state of the ligament in vivo, where the constraints of attachment to rigid bone and the force of the joint pressure lead to nonzero strain even when the spine is not loaded. In this work, we quantified these two effects using cadaveric lumbar spines (five spines, 20 total facet joints harvested from L2 to L5). The effect of joint pressure was measured by injecting saline into the joint space and tracking the 3D capsule surface motion via digital image correlation, and the prestrain due to attachment was measured by dissecting a large section of the tissue from the bone and by tracking the motion between the on-bone and free states. We measured joint pressures of roughly 15–40 kPa and local first principal strains of up to 25–50% when 0.3 mL of saline was injected into the joint space; the subsequent increase in pressure and strain were more modest for further increases in injection volume, possibly due to leakage of fluid from the joint. The largest stretches were in the bone-to-bone direction in the portions of the ligament spanning the joint space. When the ligament was released from the vertebrae, it shrank by an average of 4–5%, with local maximum (negative) principal strain values of up to 30%, on average. Based on these measurements and previous tests on isolated lumbar facet capsular ligaments, we conclude that the normal in vivo state of the facet capsular ligament is in tension, and that the collagen in the ligament is likely uncrimped even when the spine is not loaded. [DOI: 10.1115/1.4053993]

Introduction

The lumbar facet capsular ligament, which contributes to the health and stability of the lumbar spine, connects adjacent vertebrae by spanning between, and fully encapsulating, the superior articular process of the inferior vertebra and the inferior articular process of the superior vertebra. The interfacing surfaces of the articular processes are covered with cartilage and are lubricated by the synovial fluid contained within the joint space. The articular processes, along with the synovium and synovial fluid, are considered the compressive load bearers of the joint, while the fibrous facet capsular ligament limits motion by resisting tensile loads [1–3]. The lumbar facet joints were previously reported [4] to bear 3–25% of a compressive load applied to the spine, such as body weight, with the remainder being shared by the intervertebral disk. The collagen fibers found within the facet capsular ligament's microstructure are highly aligned with a primary orientation in the bone-to-bone direction [5]. These collagen fibers are load-bearing under tension and are believed to help maintain spinal health by restricting harmful translations and rotations of adjacent vertebrae [2,6].

Although the facet capsular ligament has been recognized as a possible source of low back pain for over a century [7], prior low back pain research has focused primarily on the intervertebral disk. To date, mechanical testing of the lumbar facet capsular ligament has been limited to planar mechanical tests of excised, off-bone samples, such as uniaxial [2], biaxial [6], or shear [8] testing. The facet capsular ligament's structural-mechanical relationship has been well defined with these tests, with key observations having been made about fiber alignment and measured tissue stiffness. Briefly, the mechanical response of the facet capsular ligament is nonlinear when stretched parallel to the primary collagen fiber alignment. There is a long toe region within which the elastin component may dominate the tissue's response while the collagen fibers remain crimped and unloaded [2,6,9]. In contrast, the ligament is more linear and more compliant in the transverse direction, and shear tests provide evidence of off-angle fibers contributing to the tissue's mechanics [8]. For these traditional planar mechanical tests, the facet capsular ligament is cut off the bone and flattened prior to testing, and it is not clear that the unloaded state of the free ligament is relevant to the in vivo, on-bone state. As a result, it is difficult to interpret the strain fields of the facet capsular ligament during physiologic motion [10] and to specify correctly the ligament state in whole-motion-segment finite element models [11]. For example, the facet joint capsule may be pressurized due to the encapsulation of the synovial fluid within the joint cavity. Although there has been limited research on the pressure within in vivo facet capsular joints, previous studies on the contact pressure of adjacent articular facet surfaces of the lumbar spine observed peak contact pressures of up to 6.1 MPa on the dorsal region of the articular cartilage during combined loading [1]. A further study of contact pressure within the cervical spine observed mean contact pressures of 158 kPa during extension, with measured contact pressure varying across the articular surface [1,12]. However, these studies do not consider the increase in contact pressure due to the fluid pressure alone. Additionally, these studies do not account for pressure increases during rapid, high load dynamic motions due to the relative incompressibility of the synovial fluid and little time for it to permeate out of the capsule space to retain baseline pressure. Further analysis on the strain contribution of pressurized facet capsular ligaments may help further our understanding of how facet joint effusions can lead to degenerative pathologies, such as spondylolisthesis [13].

In this study, we considered two factors so as to address the limited knowledge of the on-joint mechanical state:

(1) *Joint pressurization* via the encapsulated synovial fluid, measured by an inflation experiment on an intact cadaveric facet joint, and

Manuscript received November 29, 2021; final manuscript received February 25, 2022; published online March 24, 2022. Assoc. Editor: Ian A. Sigal.

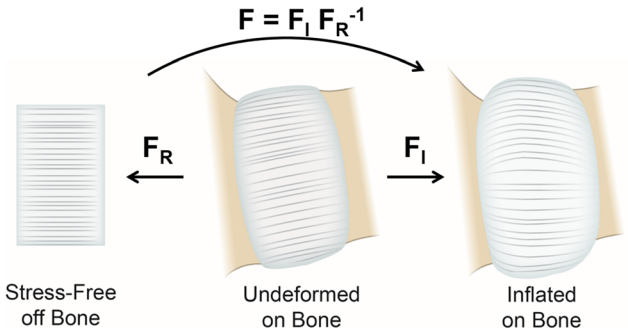

Fig. 1 Posterior view of the facet capsular ligament in a stress-free state, the unloaded on-bone state, and the inflated state. The total deformation (*F*) of the ligament from its stress-free configuration is the combined deformation of the residual and inflated states.

(2) *Residual strain* in the ligament due to its attachment to the vertebrae, addressed by a study of deformation when the ligament is released from the bone.

Methods

Sample Preparation. Five donor lumbar spines (31M, 41F, 46M, 71M, 73F) were obtained through the Anatomy Bequest Program at the University of Minnesota, Twin Cities. Twenty facet capsular samples, from a variety of lumbar levels (L2–L5) and from both the left and right portion of the spine, were obtained from the donor spines. Each spine was scanned in a 3T MRI (Siemens MAGNEtoM Prisma) at the University of Minnesota Center for Magnetic Resonance Research, and the health of the facet joint was graded on the Fujiwara scale [14]. The spine was cleared of the surrounding soft tissue to expose the posterior region of both the left and right L2–L5 facet capsular ligaments. To prepare the samples for strain tracking via digital image correlation, dried powdered Verhoeff-Van Gieson stain was used to speckle the surface of the facet capsular ligament samples [6,8].

Inflation Testing. Each facet joint specimen ($n = 20$) was injected with approximately 0.55 mL of 1% phosphate-buffered saline (PBS) at a rate of 1 mL/min by passing a needle (outer diameter of 0.53 mm) through the ligament and into the joint space between adjacent facet pairs. The chosen needle gauge was confirmed to be sufficiently small to pass into the joint space between adjacent articular processes by acquiring X-ray images of a representative sample (Supplemental Fig. 1 available in the Supplemental Materials on the ASME Digital Collection). A pressure transducer (Harvard Apparatus) measured the pressure within the joint space for a given volume of injected PBS, and a baseline pressure drop due to flow through the needle was established prior to insertion into the joint space and subtracted from the measurement. The PBS was withdrawn from the joint space at the conclusion of the test to return the facet capsular ligament to its original, uninflated state and to prepare the sample for the residual strain test. Speckle displacements were tracked over the course of the experiment using open-source three-dimensional (3D) strain-tracking software [15]; details can be found below in the section *3D Strain Tracking*.

Residual Strain Testing. Following inflation testing, the facet capsular ligament was cut into a rectangular sample using a 15-blade scalpel, with the longer edge cuts occurring parallel to the spinous process (superior–inferior axis) and the shorter edge cuts occurring along the medial-lateral axis. Careful consideration was taken to prevent speckle smearing and to release the underside (anterior) of the ligament fully from the bone. The deformation of the ligament due to the release of the residual strain was continuously tracked in 3D.

Three-Dimensional Strain Tracking. Facet capsular ligament surface displacement was tracked in 3D using a three-camera stereo system (Canon EOS Rebel T3i with Canon 100 mm f/2.8 Macrolens, Canon EOS Rebel T3i with Canon 18–55 mm f/3.5–5.6 lens, and Canon EOS Rebel T2i with Canon 105 mm Macrolens, Huntington, NY) with stereo planes of 15 deg between adjacent camera pairs. A focal distance was chosen such that the entire sample was within the camera's field of view. Camera hardware parameters are provided in the Supplemental Materials on the ASME Digital Collection. Each camera recorded at 1920 × 1280 30fps, and videos were synced using an audio cue in Cyberlink PowerDirector 19.

A quarter-cylinder calibration object with a known, uniform speckling pattern was used to calibrate the three-camera system. The calibration object was placed on top of the sample and within the field of view of each camera at the start of testing. The calibration images were then analyzed, using 3D digitial image correlation [15], to relate the positions of the calibration pattern within the image to its known position in 3D space. This step also served to relate the positioning of the three cameras relative to one another with the calibration outputs. Reconstruction errors were calculated, and, due to incompatible overlap between adjacent camera pairs, the camera pair resulting in the lowest reconstruction error was chosen for further analysis. Samples with reconstruction errors under 10% were considered for further analysis.

Ligament strains were also analyzed using 3D digitial image correlation, which initially uses the open-source, subset based two-dimensional (2D) strain tracking software NCorr [16], to calculate the speckle displacement from stereo-image pairs before a 3D reconstruction algorithm computes full-field 3D ligament displacement, surface strains, and other rigid-body motion. For the 2D portion of the analysis, a region of interest (ROI) was selected to include the released area and the area immediately surrounding it. Each ROI is discretized based on the specified subset size and spacing, and points correlated between images are triangulated into individual elements within the ROI. For inflation analysis, a subset size of 26 pixels and a subset spacing of 13 pixels was chosen for each sample. For residual strain analysis, a subset size of 40 pixels and a subset spacing of 20 pixels were chosen. Additionally, a backward analysis was conducted on the residual strain to ensure that the chosen region of interest included only the portion of the ligament that was released from the bone. These subset sizes and spacing ensured that 3–5 speckles were viewed within the subset's region. The image dataset for the residual strain analysis included the same image of the undeformed sample, prior to inflation testing, as the inflation analysis image dataset. This process ensured that the deformations from each test were related back to the same undeformed, reference ligament configuration. All strains reported in this study are Green–Lagrangian strains.

Some portions of the ROI were untrackable due to a high normalized correlation coefficient between the tracked stereo images. A cutoff correlation coefficient of 0.7 was chosen to remove outliers due to bad tracking. Both increasing and decreasing area changes were observed in some samples. For this reason, the mean area change for a sample was calculated over the middle portion of the tracked ROI.

Analysis—Inflation Testing. Nine facet capsular ligament samples that leaked were removed from the inflation testing analysis, leaving a total of 11 facet capsular ligament samples taken from different lumbar motion segments (L2–L5). A relationship between inner capsular pressure and volume of injected saline was found for each inflated sample. For each point along the pressure–volume curve, the maximum area change was calculated for each sample as the largest surface Jacobian of the elements within the sample's strain-tracked region of interest that successfully tracked over the entire testing time span. Additionally, the maximum first principal strains (i.e., the largest eigenvalue of the strain tensor) were measured for the point at which the maximum area change occurs. An angle of the first principal strain was calculated in reference to the medial-lateral axis of the sample as the dot product of the first principal strain vector with the global

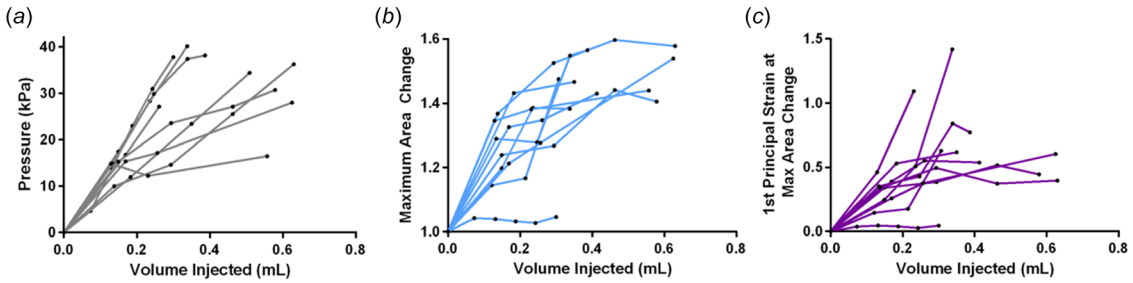

Fig. 2 (*a*) The pressure–volume relationship of the capsular joint space of all inflated samples, (*b*) the maximum area change versus volume of injected saline for each sample, and (*c*) the first principal strain at the location of maximum area change versus volume of injected saline

medial-lateral axis. A positive angle is defined as clockwise toward the superior direction of a given sample. To represent more clearly the deformation of the ligament in 3D space during inflation, the 2D change in curvature for the ligament was also calculated. An estimate of the facet joint location was obtained by overlaying the 3D ligament surface obtained from strain tracking onto the segmented bone geometries for each representative sample.

Analysis—Residual Strain Testing. The mean surface area change during the residual strain test was calculated as the determinant of the resulting surface deformation gradient tensor from 3D strain tracking. The mean area change was calculated for all elements in the tracked ROI as well as for the center portion of the tracked ROI. As in the inflation tests, the center portion was examined to reduce the influence of any outlier elements on the outside edge of the ROI.

Analysis—Total Deformation. For the eleven samples that underwent both inflation and residual strain analysis, three deformation tensors were obtained for each discretized element on the tracked ROI related by the formula (Fig. 1)

$$\boldsymbol{F} = \boldsymbol{F}_{\boldsymbol{I}} \boldsymbol{F}_{\boldsymbol{R}}^{-1} \tag{1}$$

The three deformation gradients are as follows:

- $\boldsymbol{F}$ is the deformation from the truly unloaded tissue state to the inflated state, representing the deformation state of the facet capsular ligament on a pressurized joint with no other loading,
- $\boldsymbol{F}_{\boldsymbol{I}}$ is the deformation experienced by the facet capsular ligament on the joint from the uninflated to the inflated state, and
- $\boldsymbol{F}_{\boldsymbol{R}}^{-1}$ is the deformation form the truly unloaded tissue state to the uninflated on-joint state. This tensor is the inverse of the deformation gradient calculated when the tissue was released from the bone.

Statistical Analysis. The relationship between the area change when maximally inflated and the area change when release during the residual strain test was determined by plotting each area change for a given element on the tracked ROI. Linear regression was performed to determine the relationship and its significance. This process was repeated to determine the relationship between first principal strain during inflation and first contractile strain upon release. All values are shown as mean ± 95% confidence interval.

Comparison to Facet Capsular Strains During Physiological Motion. For a better understanding of the contribution of joint pressurization and residual strain on total ligament strain, the principal strains during flexion reported by Ianuzzi et al. [10] were recalculated to include both contributions. The global coordinate system was chosen to match [10] where E_1 during flexion was observed to most closely align in the medial-lateral direction and E_2 in the superior-inferior direction. A representative element within the tracked ROI was chosen from the representative sample 1 and used for the analysis. The total deformation tensor accounting for joint motion, inflation, and residual strain was obtained by the following:

$$\boldsymbol{F}_{\boldsymbol{T}} = \boldsymbol{F}_{\boldsymbol{M}} \boldsymbol{F}'_{\boldsymbol{I}} \boldsymbol{F}'^{-1}_{\boldsymbol{R}} \tag{2}$$

The four deformation gradients are as follows:

- $\boldsymbol{F}_{\boldsymbol{T}}$ is the deformation from the undeformed state to the inflated state with joint motion, representing the deformation state of the facet capsular ligament on a pressurized joint with physiological motion,
- $\boldsymbol{F}_{\boldsymbol{M}}$ is the deformation experienced during flexion for a left L3L4 motion segment, calculated from Ref. [10],
- $\boldsymbol{F}'_{\boldsymbol{I}}$ is the deformation experienced from the uninflated to the inflated state with an injected volume of 0.5 mL, and rotated into the coordinate system described in Ref. [10].
- $\boldsymbol{F}'^{-1}_{\boldsymbol{R}}$ is the deformation from the truly unloaded tissue state to the uninflated on-joint state. This tensor is rotated from its local coordinate system into the global coordinate system described in Ianuzzi, et al. [10]

The Green–Lagrangian strain tensor was then calculated from $\boldsymbol{F}_{\boldsymbol{T}}$. E_1 is the largest eigenvalue and E_2 was the smallest eigenvalue of the strain tensor.

Results

Inflation of the Joint Space. Contrary to the nonlinear behavior of off-bone planar samples, pressure within the joint space increased linearly with volume for most samples, but there were some samples that exhibited an initial linear increase in pressure with volume before tapering off (Fig. 2(*a*)). This sublinear response may have been due to minor leakage of the joint fluid or a shift in the facet joints that relieved some of the pressure. Despite a variance in the lumbar spine levels, ranging from L2–L3 to L4–L5, of the facet capsules studied, most samples had very similar initial slopes. For injected volumes up to 0.25 mL, the volumetric compliance (i.e., the inverse slope of the lines in Fig. 2(*a*)) over the samples was 0.011 ± 0.0018 mL/kPa (mean ± 95% confidence interval). The maximum local area change (Fig. 2(*b*)) and first principal strain at maximum area change (Fig. 2(*c*)) showed considerably more spread.

Looking into three representative samples in more detail, we can see that the greatest principal strains are observed in two locations: (1) the portion of the ligament spanning across the joint gap and (2) the portion of the ligament at the enthesis (Fig. 3). A rough estimate of the bone location under the facet capsular ligament is shown in Fig. 3(*a*1–*a*3). This effect is most clearly shown in sample 1 (Fig. 3(*a*1, *b*1, and *d*1)). The direction of the first principal strain is generally in the bone-to-bone direction (Fig. 3(*b*1)), which ranges from 15 to 70 deg in the axial plane in the lumbar spine, with larger angles toward the lower L4–L5 spine region

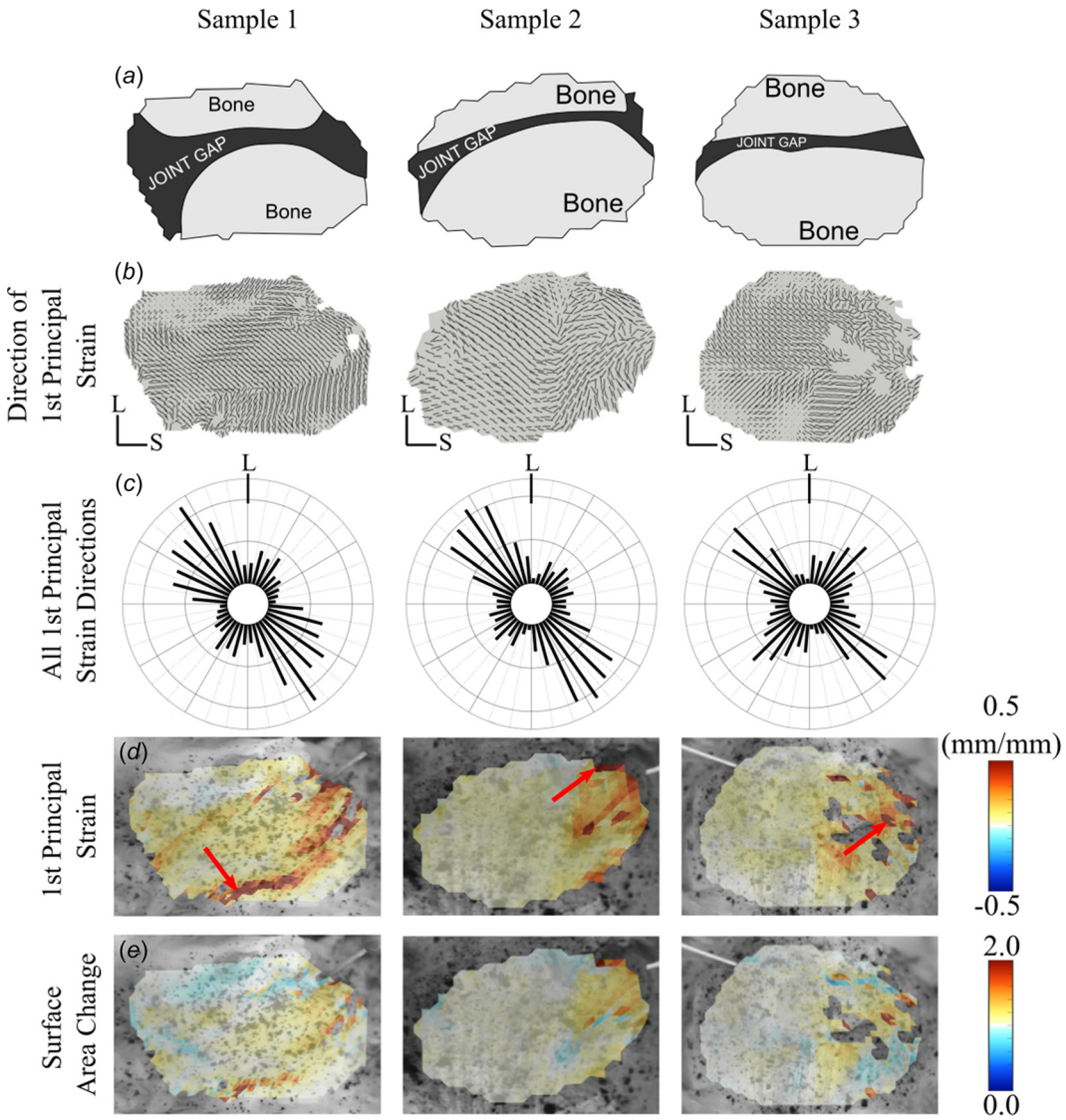

Fig. 3 (*a*) The location of the facet joint within the ROI estimated from the overlay of the tracked ROI onto CT segmentation of three representative samples. (*b* and *c*) The direction of and (*d*) the maximum principal strain fields at maximum inflation for three representative samples. The angles shown in (*c*) are the principal direction with respect to the medial-lateral axis of a sample. Arrows denote the location of maximum strain. Samples 1 and 2 are from the left side. Sample 3 is from the right side; images of sample 3 are mirrored for easier comparison to samples 1 and 2. The needle tip for each sample can be seen in the upper right corner of each image for sample 1 and 2 and in the upper left corner of the image for sample 3. Axes denote the superior (S) and lateral (L) direction for each sample. (*e*) The surface area change at maximum inflation.

[1,17]. In the case of sample 1, the first principal strain is oriented from bone-to-bone. Similarly, although to a lesser degree, the same trend is observed in sample 2 (Fig. 3(*b*3 and *d*3)). Here, the maximum first principal strain is observed in the portion of the ligament spanning the joint gap and closest to the site of needle insertion. The direction of max first principal strain (Fig. 3(*b*2 and *b*3)) is oriented bone-to-bone in the region with the highest first principal strain (Fig. 3(*d*2 and *d*3)).

Figure 4(*a*) displays the location of two slices taken from the 3D strain tracking results of sample 1. One slice runs roughly bone to bone and the other along a bone surface. The greatest change in the surface contour is observed in the portion of the ligament that spans across the joint gap (Figs. 4(*b*) versus 4(*c*)). This region initially inflates outward before a pressure threshold is surpassed, at which point the two facet surfaces move away from each other, and the joint gap is further inflated. The behavior is reflected in the slices at three pressures: (1) uninflated at $P = 0$ kPa, (2) outward inflation at $P = 10$ kPa, and (3) outward inflation with facet motion at $P = 36$ kPa. A slice along the joint shown in Fig. 4(*c*) shows different behavior. The slice, taken close to the enthesis of the facet capsular ligament, exhibits very little deformation. For this representative sample, the change in curve length at maximum inflation with facet motion, when the pressure $= 36$ kPa, in the bone- to-bone direction is $+4.63\%$ compared to -1.46% along the joint direction.

Summarizing the inflation results, we saw a nearly linear pressure–volume relationship for the joint space during inflation, with a heterogeneous strain field arising in the facet capsular ligament. The largest principal strains, which were of the order of 50% for a joint volume of 0.3 mL for most samples, occurred in the region of the facet capsular ligament above the joint space and in the bone-to-bone direction.

Release of Residual Strains. Viewed grossly, the facet capsular ligament shrank upon release from its attachments to the vertebrae. The area change upon release is shown in Fig. 5 for the

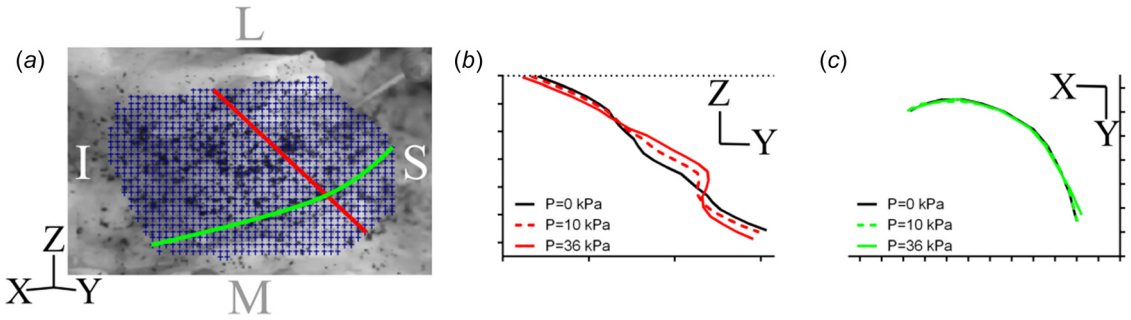

Fig. 4 Anatomy is as described in Figs. 3(*a*)–3(*c*). (*a*) En face image of sample 1 (same as Fig. 3(*a*)) with lines drawn in the bone-to-bone (L-M direction) and along-bone (S-I direction) direction. (*b*) Surface contour along bone-to-bone line shows motion upon outward inflation ($P = 10$ kPa) and inflation with facet motion ($P = 36$ kPa). (*c*) Along-bone line shows no significant motion because of anchorage to the bone. The superior (*S*), inferior (*I*), medial (*M*), and lateral (*L*) are shown on the representative sample in panel A. Tick spacing in panel B and C is 2 mm.

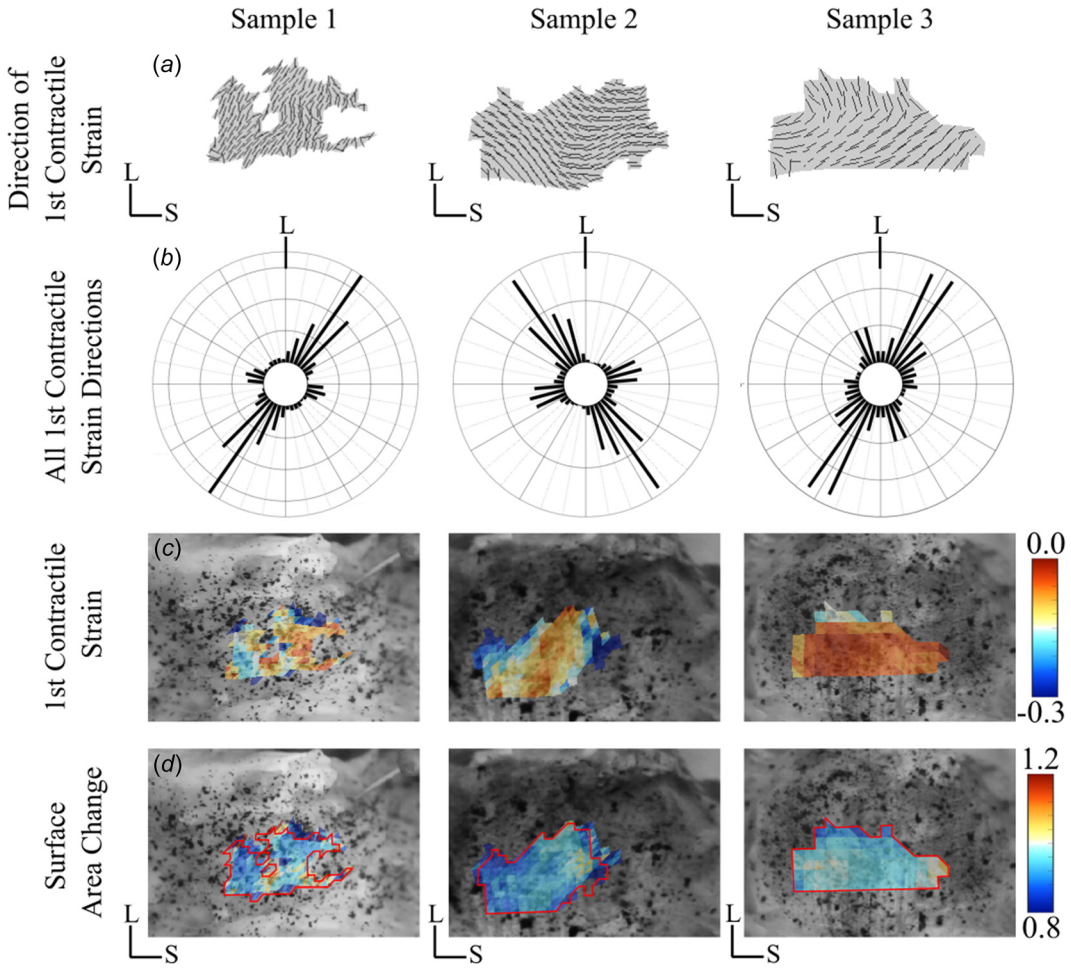

Fig. 5 (*a* and *b*) The direction and (*c*) magnitude of the first contractile strain, measured as the most negative eigenvalue of the strain tensor and its corresponding eigenvector, of the same three representative samples shown in Fig. 3. The angles shown in (*b*) are the component of the first contractile strain vector with respect to the medial-lateral axis of the sample. (*d*) The surface area change across the tracked ROI for the residual strain test. Area change and first contractile strain are shown in 2D on the undeformed sample surface. The outline in (*d*). Depicts the size and shape of the undeformed ROI for each of the three samples. Axes denote the superior (*S*) and lateral (*L*) direction for each sample.

same samples as in Fig. 3. To avoid confusion, in this section and in Fig. 5, we use the phrase "first contractile strain" to mean the more negative of the two eigenvalues of the strain tensor, and its corresponding eigenvector. There was no clear primary direction of contraction, with the majority of contraction upon release occurring in the bone-to-bone (Fig. 5(*a*1)) or along-bone (Fig. 5(*a*2)) direction. Tissue retraction was roughly uniform, with first contractile strain values mostly in the range −0.05 to −0.1%

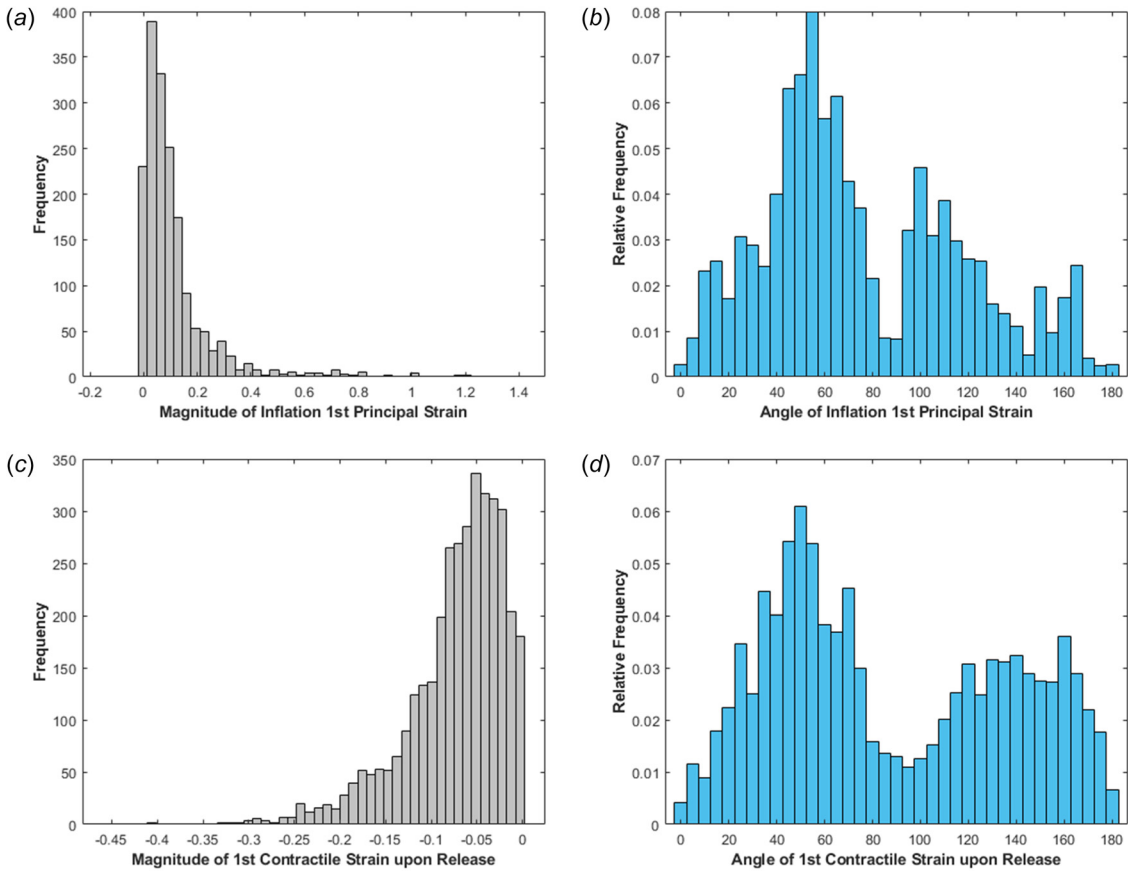

Fig. 6 The distributions of the (*a*) magnitude and (*b*) direction with respect to the medial-lateral axis of the first principal strain during inflation for all samples. Similarly, the distributions of the (*c*) magnitude and (*d*) direction, with respect to the medial-lateral axis, of the first contractile strain upon release for all samples. The direction of the inflation and residual strain vectors are weighted by the element's magnitude of the strain and normalized to the total magnitude of all samples.

(Fig. 5(*c*1–*c*3)) Similar behavior was seen in the area change (Fig. 5(*d*1–*d*3)) with values in the range of 0.9–1. The red outline in Fig. 5(*d*1–*d*3) depicts the same tracked ROI in its undeformed state. When tissue contraction was particularly small, as observed in sample 3, the edges of the undeformed ROI almost perfectly overlap with those of the deformed ROI (Fig. 5(*d*3)). Sample 1 showed nonuniform area change with higher measurements found at the edge of the tracked ROI, possibly due to edge effects that were not resolved with the correlation coefficient (Fig. 5(*d*1)). Both samples 2 and 3 appear to have a uniform area change across the surface of each ligament (Fig. 5(*d*2 and *d*3)) with mean area changes of 0.910 and 0.957 for all tracked points in the ROI, respectively.

The distribution of the first principal strains during inflation and the first contractile strains upon release for all samples is shown in Fig. 6. The direction of the principal and contractile strain is the angle off the medial-lateral axis, which is taken as being the bone-to-bone direction, with a positive angle behind defined toward the superior axis for a given sample. The average first principal strains for the tracked elements within all samples was 0.11 ± 0.0070 mm/mm (Fig. 6(*a*)), with a predominate alignment ± 55 deg off of the medial-lateral axis (Fig. 6(*b*)). The average magnitude of first contractile strain for all tracked elements in all samples was -0.078 ± 0.0019 mm/mm (Fig. 6(*c*)). The first contractile strains were less aligned, with a peak angle of 50 deg off the medial-lateral axis but with a relatively high frequency of strains aligned between 120 deg and 160 deg (Fig. 6(*d*)).

Figure 7 shows a summary of the area change, first principal strain, and first contractile strain for all samples. The mean area change over all tracked points within the ROI was 0.953 ± 0.017, indicating roughly 5% area loss upon release (Fig. 7(*a*)). The average area change for elements within the middle portion of the total tracked ROI was 0.965 ± 0.016. The mean area change at maximum inflation was 1.014 ± 0.011 (Fig. 7(*b*)). Figure 7(*c*) displays the spread of all elements' area change due to residual strain and maximum inflation. Each point represents a single element within the tracked ROI for both the inflation experiment and the residual strain experiment. There was a slight positive correlation between the area change during inflation and the area change upon release ($r^2 = 0.015$, $p < 0.0001$). It appeared that portions of the facet capsular ligament that contracted more during the residual strain test had a smaller area change when inflated. However, the r^2 value is reported very close to zero, so any relationship between the two measurements may be influenced by outliers beyond the 20% area change. To eliminate the extreme values, Fig. 7(*d*) zooms in on a portion of the graph in Fig. 7(*c*). The mean max first contractile strain for all tracked points and the middle portion was -0.283 ± 0.043 and -0.223 ± 0.041, respectively (Fig. 7(*e*)), while the mean max first principal strain during inflation was 0.588 ± 0.226 (Fig. 7(*f*)). The relationship between the first contractile strain upon release and the first principal strain upon inflation for each element for all samples is shown in Fig. 7(*g*). The equation $Y = -0.048*X - 0.057$, with $r^2 = 0.003$ and P value $= 0.002$, was fit to all the data points in all samples tracked in both the residual strain test and the inflation test. There was little to no relationship between the first contractile strain and the first principal strain. Again, Fig. 7(*h*) zooms in on a portion of the graph in Fig. 7(*g*).

To summarize, the facet capsular ligament shrank upon release from the bone, with no clear primary direction of contraction. However, most samples appeared to contract either bone-to-bone or along the bone (Fig. 5(*a*1–*a*3)). Due to the anatomy of the facet

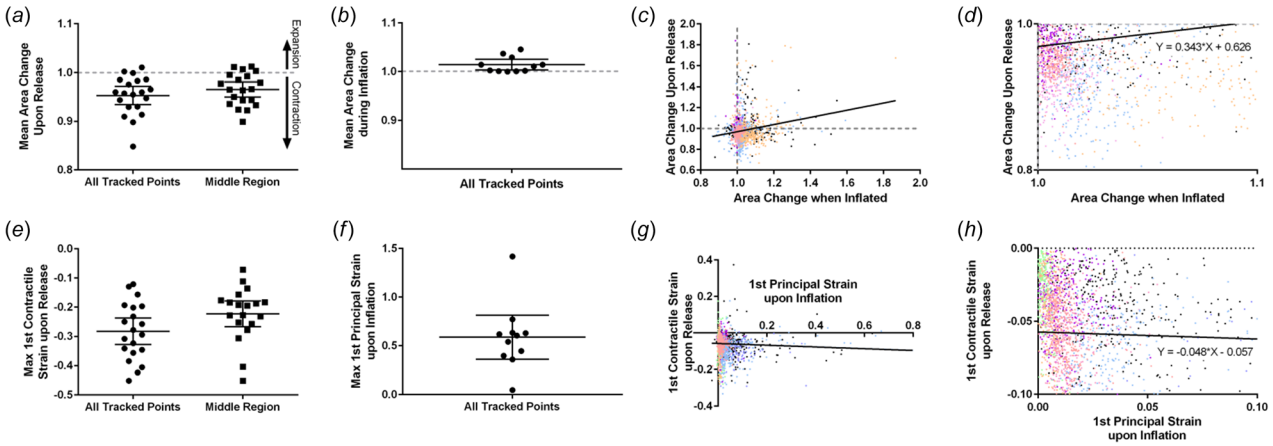

Fig. 7 (*a*) The average surface area change tracked in the ROI during the residual strain test. Both the results for all tracked points as well as points taken from the middle region of the ROI are shown. The gray line indicates no area change on release. (*b*) The average surface area change in the ROI during maximum inflation. (*c*) Plot of the area change during inflation versus the area change upon release for every element within the ROI. Only samples that inflated and released successfully are shown. (*d*) Zooms in on a region of interest of the data presented in (*c*). (*e*) The maximum first contractile strain upon release across the entire tracked ROI as well as points taken from the middle region of the ROI to reduce error due to boundary outliers. (*f*) The max first principal strain during maximum inflation and (*g*) a plot of first contractile strain during release versus first principal strain during inflation for each element with the ROI of all samples, with (*h*) a zoom in on a region of interest.

joint and the location of the joint gap within the ROI of the tracked samples, most samples were released with the majority of the ligament over and attached to the bone. Consequently, the tissue contracted about 4–5% upon release (Fig. 7(*a*)). There was neither a clear correlation between area change upon release and upon inflation (Figs. 7(*c*) and 7(*d*)) nor with the first contraction strain upon release and first principal strain upon inflation (Figs. 7(*g*) and 7(*h*)).

Total Deformation of in Situ Facet Capsular Ligament Samples. To account for the combined effect of residual strain and joint pressurization, the total deformation due to both was calculated; the results for sample 1 are shown as surface area changes in Fig. 8. To clarify, the residual surface area change is the hypothetical deformation required to take a planar, off-joint sample and place it back on the joint (Fig. 8(*a*)). This deformation gradient is calculated as the inverse of the deformation gradient tensor of the residual strain test. Due to the current absence of in situ facet capsular ligament joint capsule pressure measurements, we have shown the total deformation at three pressure levels: approximately 12 kPa (low), 22 kPa (mid), and 36 kPa (high) (Figs. 8(*b*)–8(*d*)). The residual surface area change shown in Fig. 8(*a*) appears as the dominant strain in the total strain state (Figs. 8(*b*)–8(*d*)). This may be due to less overlap between the area observed during inflation and the tracked area during the residual strain test.

Figure 9 demonstrates the change in the observed on-joint ligament strains with motion when including the joint pressurization and residual strain contribution, calculated as described under Methods in *Comparison to Facet Capsular Strains during Physiological Motion*. The black line, labeled M, is the principal strains on an on-joint left L3L4 facet capsular ligament due to flexion as measured by Ianuzzi et al. [10]. The blue line, labeled $M+I+R$, represents the principal strains on the ligament due to joint pressurization, residual strain, and joint motion. The inflation contribution, labeled I, added 20% strain in the E_1, or superior–inferior,

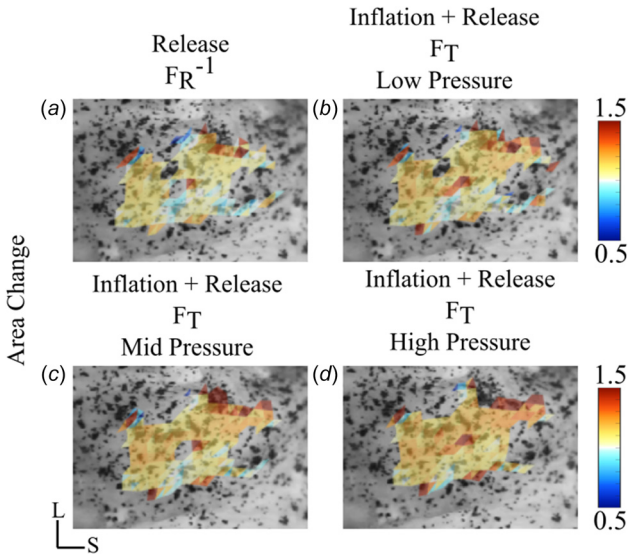

Fig. 8 The surface area change for sample 1 (*a*) needed to place the off-bone, planar ligament back on to its on-joint state, as well as the total deformation due to residual strain and pressurization to roughly (*b*) 12 kPa, (*c*) 22 kPa, and (*d*) 36 kPa are shown. All surface area changes are shown in 2D on the undeformed ligament surface.

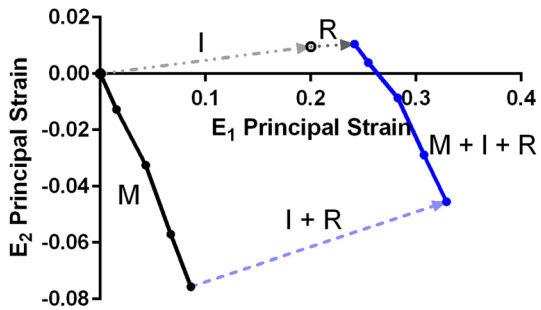

Fig. 9 E_1 and E_2 lumbar facet joint capsule strains during joint motion (*M*), residual strain (*R*), and inflation (*I*) strain for an injected volume of approximately 0.5 mL. Strains for joint motion were obtained from Ianuzzi et al. in their study of facet capsular ligament strains during flexion. The new total strain was calculated to include the contributions from joint pressurization and the residual strain, in addition to those observed on the ligament during flexion. E_1 was aligned in the medial-lateral direction and E_2 was aligned in the superior-inferior direction.

direction. The residual strain contributions, labeled R, an addition 4% strain in the E_1 direction, giving a total of 24% strain on the ligament before spinal motion. This indicates that the collagen fibers are in tension in both the E_1 (bone-to-bone) and E_2 (alone-joint) direction before the addition of spinal motions such as flexion.

Discussion

In this study, we measured the facet capsular ligament strains due to both joint pressurization and residual strain, both of which have been unaccounted for in previous studies that characterized the facet capsular ligament with planar mechanical tests. Using 3D strain tracking, we determined ligament strain at a given volume of injected saline, as well as the inner capsular pressure (Figs. 2 and 3). We also measured contraction of the ligament upon the release of the residual strain (Fig. 5). To our knowledge, this is the first study of the deformation state of the facet capsular ligament on an unloaded joint, providing a bridge between the results of previous whole lumbar spine studies [10] and traditional planar mechanical testing of isolated lumbar facet capsular ligaments [2,6,8,18,19].

The major conclusion of this study is that even when the spine is not loaded, the facet capsular ligament is under constant tensile strain due to its attachment to the bone and the influence of the joint pressure (Figs. 5 and 7). The strain is not merely a nonzero quantity but could have mechanical significance for in vivo function of the lumbar facet capsular ligament. The toe region for uniaxial loading of the lumbar facet capsular ligament is roughly 10–12% strain [2,9], and for biaxial loading it is roughly 6–8% strain [6,20], measured from the true undeformed state. These numbers are comparable to the strains we calculated for the facet capsular ligament due to prestrain and joint pressure, suggesting that the collagen fibers in the facet capsular ligament are never crimped in vivo, or perhaps only in the case of a spinal motion that would put the facet capsular ligament into compression relative to the neutral spine state. This result has bearing on whole-joint models of the lumbar spine [11,21,22] and on attempts to use in vitro experimental data to understand in vivo tissue mechanics [19,23]. For example, an analysis based on facet capsular ligament strain from its true unloaded state rather than from the neutral spine state would overestimate the facet capsular ligament laxity at low strains and thus would overestimate the range of motion for any motion restricted by the facet capsular ligament.

The range of pressures in the lumbar facet joint is, to our knowledge, unmeasured. Jaumard et al. [1,12] measured the joint pressure in the cervical facet joint, but their device measured the pressure on the cartilage surface, not the pressurization of the synovial fluid. It is conceivable that the joint pressure could be measured via an instrumented syringe during intra-articular injection for low back pain, but to our knowledge, no such measurement has been made; since such injections are typically 0.5–1.5 mL [24] it might also be possible to measure the joint pressure–volume relationship in vivo. Our cadaveric joint results showed a significant pressure rise for 0.5 ml of injection (Fig. 2), however, without knowing the in vivo pressure range of the joint capsule, the applicability of our inflation results are unknown. Our study is also limited to characterizing the truly undeformed state of the lumbar facet capsular ligament from isolated donor spine units, without musculature or body weight, which is not the true resting state in vivo. Additionally, in our study the facet joints are unconstrained which, when pressurized, may cause motions that are potentially not possible in vivo. Computationally modeling the results of our study with realistic geometries and boundary conditions may provide further insights into the significance of these limitations.

There was a great degree of variability observed in the direction of the first principal and first contractile strain (Figs. 3(*b*) and 3(*c*), 5(*a*) and 5(*b*), and 6). Some samples displayed a clear predominate direction of first principal strain, aligning roughly in the bone-to-bone direction (Figs. 3(*b*1 and *b*2)), while others had a less clear preference (Fig. 3(*b*3)). Difference in the location and direction of the highest strain in the facet capsular ligament joint gap region may be due to the increase in angle from the axial plane of the two articulating facet surfaces. The orientation angle of the two surfaces, and thus that of the joint gap, becomes more aligned in the sagittal plane further down the lumbar spine [1]. Samples 1 and 2 were both taken from the left facet capsular ligament. Sample 3, however, was taken from the right side of the spinous process. This is observed to a lesser degree in the direction of the first contractile strain upon release (Figs. 5(*a*) and 5(*b*)), however, the amount of trackable area is smaller than in inflation. While the sum distribution of all first contractile strain directions has a peak angle of 50 deg off the medial-lateral axis, a bimodal distribution is observed with strain directions occurring 100–120 deg off the medial-lateral axis with a high relative frequency (Fig. 6(*d*)). Although the overall fiber alignment is taken as being bone-to-bone, previous studies have demonstrated a high degree of heterogeneity in the local collagen fiber orientation [25]. Further studies on the relationship between the direction of the principal strains and the predominate local alignment of the collagen microstructure are needed to explain this variability and the lack of correlation seen between the first principal inflation strain and the first contractile strain (Figs. 7(*c*), 7(*d*), 7(*g*), and 7(*h*)).

Previous studies have demonstrated that planar off-bone facet capsular ligament samples are uncrimped until about 16% stretch [9]. We determined the total ligament strain from a truly unloaded, planar state to being on-joint with applied motion by adding the contributions due to joint pressurization and residual strain to the on-joint strain observation by Ianuzzi et al. [10]. We looked at the strains due to flexion for a left L3L4 sample with primary axis in the medial-lateral (E_1) direction and superior–inferior (E_2) (Fig. 9). The largest magnitude strains were those in the E_1 direction. Considering that this is roughly the bone-to-bone direction, the strains due to inflation and residual strain have the potential to uncrimp the collagen fibers fully from the truly unloaded to the on-joint state without considering an additional strain due to joint motion (Fig. 9). The collagen fibers in the facet capsular ligament on a pressurized joint are in tension before motion causing the on-joint observation of ligament strain fields to underestimate the total applied strain.

The potential role of fluid pressurization in determining the lumbar facet capsular ligament's mechanical state also suggests that one may need to consider how the available facet joint volume changes during spinal motion. If a motion causes the joint space to lose volume, and the synovial fluid cannot escape quickly, it would be expected that the fluid would pressurize and push the facet capsular ligament out so as to maintain volume; a similar but opposite effect would be seen if the joint space volume were increased, possibly creating a negative (suction) pressure and pulling the facet capsular ligament into the joint space. If the configuration were maintained for an extended period of time, however, synovial fluid turnover could allow re-equilibration of the joint pressure within the facet capsular ligament.

The potential role of pressurization also compels some discussion of the anatomy of the lumbar facet capsular ligament, which contains an inner elastin-rich layer and an outer collagen-rich layer [5,9]. By analogy with arterial wall mechanics, we can hypothesize that the elastin component provides elastic restoration under small loads, such as might arise due to synovial fluid pressurization during normal motions, and the collagen component provides stiffness resistance to pressure overload, due to abnormal motions. This hypothesis could be explored in various ways, including leveraging the large volume of work and methodological development for arterial mechanics.

Acknowledgment

Tissue samples were obtained through the University of Minnesota Anatomy Bequest Program. The authors thank Lily Kollitz, Catherine Lee, and Milagros Fernandez Oromendia for their assistance.

Funding Data

- National Institutes of Health (Grant Nos. T32-AR050938 and U01-010326; Funder ID: 10.13039/100000002).

References

[1] Jaumard, N. V., Welch, W. C., and Winkelstein, B. A., 2011, "Spinal Facet Joint Biomechanics and Mechanotransduction in Normal, Injury and Degenerative Conditions," ASME J. Biomech. Eng., **133**(7), p. 071010.
[2] Little, J. S., and Khalsa, P. S., 2005, "Material Properties of the Human Lumbar Facet Joint Capsule," ASME J. Biomech. Eng., **127**(1), pp. 15–24.
[3] Adams, M. A., and Hutton, W. C., 1983, "The Mechanical Function of the Lumbar," Spine (Phila. Pa. 1976), **8**(3), pp. 327–330.
[4] Yang, K. H., and King, A. I., 1984, "Mechanism of Facet Load Transmission as a Hypothesis for Low-Back Pain," Spine (Phila. Pa. 1976), **9**(6), pp. 557–565.
[5] Yamashita, T., Minaki, Y., Özaktay, A. C., Cavanaugh, J. M., and King, A. I., 1996, "A Morphological Study of the Fibrous Capsule of the Human Lumbar Facet Joint," Spine (Phila. Pa. 1976), **21**(5), pp. 538–543.
[6] Claeson, A. A., and Barocas, V. H., 2017, "Planar Biaxial Extension of the Lumbar Facet Capsular Ligament Reveals Significant in-Plane Shear Forces," J. Mech. Behav. Biomed. Mater., **65**, pp. 127–136.
[7] Cohen, S. P., and Raja, S. N., 2007, "Pathogenesis, Diagnosis, and Treatment of Lumbar Zygapophysial (Facet) Joint Pain," Anesthesiology, **106**(3), pp. 591–614.
[8] Bermel, E. A., Thakral, S., Claeson, A. A., Ellingson, A. M., and Barocas, V. H., 2020, "Asymmetric in-Plane Shear Behavior of Isolated Cadaveric Lumbar Facet Capsular Ligaments: Implications for Subject Specific Biomechanical Models," J. Biomech., **105**, p. 109814.
[9] Gacek, E., Bermel, E. A., Ellingson, A. M., and Barocas, V. H., 2021, "Through-Thickness Regional Variation in the Mechanical Characteristics of the Lumbar Facet Capsular Ligament," Biomech. Model. Mechanobiol., **20**(4), pp. 1445–1457.
[10] Ianuzzi, A., Little, J. S., Chiu, J. B., Baitner, A., Kawchuk, G., and Khalsa, P. S., 2004, "Human Lumbar Facet Joint Capsule Strains: I. During Physiological Motions," Spine J., **4**(2), pp. 141–152.
[11] Bermel, E. A., Barocas, V. H., and Ellingson, A. M., 2018, "The Role of the Facet Capsular Ligament in Providing Spinal Stability," Comput. Methods Biomech. Biomed. Eng., **21**(13), pp. 712–721.
[12] Jaumard, N. V., Bauman, J. A., Welch, W. C., and Winkelstein, B. A., 2011, "Pressure Measurement in the Cervical Spinal Facet Joint: Considerations for Maintaining Joint Anatomy and an Intact Capsule," Spine (Phila. Pa. 1976), **36**(15), pp. 1197–1203.
[13] Chaput, C. D., Allred, J. J., Pandorf, J. J., Song, J., and Rahm, M. D., 2013, "The Significance of Facet Joint Cross-Sectional Area on Magnetic Resonance Imaging in Relationship to Cervical Degenerative Spondylolisthesis," Spine J., **13**(8), pp. 856–861.
[14] Fujiwara, A., Tamai, K., Yamato, M., An, H. S., Yoshida, H., Saotome, K., and Kurihashi, A., 1999, "The Relationship Between Facet Joint Osteoarthritis and Disc Degeneration of the Lumbar Spine: An MRI Study," Eur. Spine J., **8**(5), pp. 396–401.
[15] Solav, D., Moerman, K. M., Jaeger, A. M., Genovese, K., and Herr, H. M., 2018, "MultiDIC: An Open-Source Toolbox for Multi-View 3D Digital Image Correlation," IEEE Access, **6**, pp. 30520–30535.
[16] Blaber, J., Adair, B., and Antoniou, A., 2015, "Ncorr: Open-Source 2D Digital Image Correlation Matlab Software," Exp. Mech., **55**(6), pp. 1105–1122.
[17] Panjabi, M. M., Oxland, T., Takata, K., Goel, V., Duranceau, J., and Krag, M., 1993, "Articular Facets of the Human Spine:Quantitative Three-Dimensional Anatomy," Spine (Phila. Pa. 1976), **18**(10), pp. 1298–1310.
[18] Little, J. S., and Khalsa, P. S., 2005, "Human Lumbar Spine Creep During Cyclic and Static Flexion: Creep Rate, Biomechanics, and Facet Joint Capsule Strain," Ann. Biomed. Eng., **33**(3), pp. 391–401.
[19] Ban, E., Zhang, S., Zarei, V., Barocas, V. H., Winkelstein, B. A., and Picu, C. R., 2017, "Collagen Organization in Facet Capsular Ligaments Varies With Spinal Region and With Ligament Deformation," ASME J. Biomech. Eng., **139**(7), p. 071009.
[20] Nagel, T. M., Hadi, M. F., Claeson, A. A., Nuckley, D. J., and Barocas, V. H., 2014, "Combining Displacement Field and Grip Force Information to Determine Mechanical Properties of Planar Tissue With Complicated Geometry," ASME J. Biomech. Eng., **136**(11), p. 114501.
[21] Ellingson, A. M., Shaw, M. N., Giambini, H., and An, K. N., 2016, "Comparative Role of Disc Degeneration and Ligament Failure on Functional Mechanics of the Lumbar Spine," Comput. Methods Biomech. Biomed. Eng., **19**(9), pp. 1009–1018.
[22] Zarei, V., Dhume, R. Y., Ellingson, A. M., Barocas, V. H., Zarei, V., Dhume, R. Y., and Ellingson, A. M., 2018, "Multiscale Modelling of the Human Lumbar Facet Capsular Ligament: Analysing Spinal Motion From the Joint to the Neurons," J. R. Soc. Interface, **15**(148), p. 20180550.
[23] Zarei, V., Zhang, S., Winkelstein, B. A., and Barocas, V. H., 2017, "Tissue Loading and Microstructure Regulate the Deformation of Embedded Nerve Fibres: Predictions From Single-Scale and Multiscale Simulations," J. R. Soc. Interface, **14**(135), p. 20170326.
[24] Cohen, S. P., Bhaskar, A., Bhatia, A., Buvanendran, A., Deer, T., Garg, S., Hooten, W. M., Hurley, R. W., Kennedy, D. J., McLean, B. C., Moon, J. Y., Narouze, S., Pangarkar, S., Provenzano, D. A., Rauck, R., Sitzman, B. T., Smuck, M., Van Zundert, J., Vorenkamp, K., Wallace, M. S., and Zhao, Z., 2020, "Consensus Practice Guidelines on Interventions for Lumbar Facet Joint Pain From a Multispecialty, International Working Group," Reg. Anesth. Pain Med., **45**(6), pp. 424–467.
[25] Zarei, V., Liu, C. J., Claeson, A. A., Akkin, T., and Barocas, V. H., 2017, "Image-Based Multiscale Mechanical Modeling Shows the Importance of Structural Heterogeneity in the Human Lumbar Facet Capsular Ligament," Biomech. Model. Mechanobiol., **16**(4), pp. 1425–1438.